Platelets Drive Thrombus Propagation in a Hematocrit and Glycoprotein VI–Dependent Manner in an In Vitro Venous Thrombosis Model

Marcus Lehmann, Rogier M. Schoeman, Patrick J. Krohl, Alison M. Wallbank, Joseph R. Samaniuk, Martine Jandrot-Perrus, Keith B. Neeves

Objective—The objective of this study was to measure the role of platelets and red blood cells on thrombus propagation in an in vitro model of venous valvular stasis.

Approach and Results—A microfluidic model with dimensional similarity to human venous valves consists of a sinus distal to a sudden expansion, where for sufficiently high Reynolds numbers, 2 countercurrent vortices arise because of flow separation. The primary vortex is defined by the points of flow separation and reattachment. A secondary vortex forms in the deepest recess of the valve pocket characterized by low shear rates. An initial fibrin gel formed within the secondary vortex of a tissue factor–coated valve sinus. Platelets accumulated at the interface of the fibrin gel and the primary vortex. Red blood cells at physiological hematocrits were necessary to provide an adequate flux of platelets to support thrombus growth out of the valve sinus. A subpopulation of platelets that adhered to fibrin expose phosphatidylserine. Platelet-dependent thrombus growth was attenuated by inhibition of glycoprotein VI with a blocking Fab fragment or D-dimer.

Conclusions—A 3-step process regulated by hemodynamics was necessary for robust thrombus propagation: First, immobilized tissue factor initiates coagulation and fibrin deposition within a low flow niche defined by a secondary vortex in the pocket of a model venous valve. Second, a primary vortex delivers platelets to the fibrin interface in a red blood cell–dependent manner. Third, platelets adhere to fibrin, activate through glycoprotein VI, express phosphatidylserine, and subsequently promote thrombus growth beyond the valve sinus and into the bulk flow.

Visual Overview—An online visual overview is available for this article. **(*Arterioscler Thromb Vasc Biol*. 2018;38: 1052-1062. DOI: 10.1161/ATVBAHA.118.310731.)**

Key Words: blood platelets ■ erythrocytes ■ hematocrit ■ hemorheology ■ phosphatidylserines

The initiation and propagation of venous thrombosis (VT) are poorly characterized compared with arterial thrombosis.[1] This is due, in part, to the lack of animal and in vitro models that replicate the hemodynamics and microenvironment of venous valves where most VT in humans originates. The most common animal models of VT are initiated via partial or total ligation of vessels like the inferior vena cava that do not have valves.[2,3] In vitro flow chambers are often used to simulate the flows and forces that regulate thrombus formation in straight or stenotic channels, but few recreate the geometry of venous valves.[4–6] In this study, we describe a scaled model of human venous valves that recreates their essential hemodynamics to determine the influence of blood flow, red blood cells (RBC), and platelets on thrombus propagation initiated by immobilized TF (tissue factor).

See accompanying editorial on page 980

VT is thought to result from a combination of flow stasis, hypoxia-induced activation of the endothelium, and subsequent accumulation of procoagulant factors in the valve sinus.[7,8] Flow stasis broadly refers to a complete lack of blood flow but also disturbed flows that result in low flow niches. Venous valve stasis caused by aging and immobility reduces blood flow into and within the valve sinus.[9] These unusual hemodynamic conditions in the valve sinus yield a hypoxic environment that results in the presentation of P- and E-selectin and von Willebrand factor on endothelial cells,[10] which in turn supports adhesion of blood cells and microparticles.[11] Accumulation of TF-positive microparticles, monocytes, and platelets initiates coagulation through the extrinsic pathway.[1] The intrinsic pathway may also play a role in thrombus propagation via exposure of neutrophil extracellular traps.[11] Computational models of VT suggest that a threshold quantity of TF must accumulate before the initiation of coagulation.[12] However, after this initiation, the biophysical mechanisms that regulate the propagation of a thrombus into the lumen of the vein are yet to be quantified.

Received on: April 12, 2017; final version accepted on: February 6, 2018.

From the Chemical and Biological Engineering Department, Colorado School of Mines, Golden (M.L., R.M.S., P.J.K., A.M.W., J.R.S., K.B.N.); Laboratory of Vascular Translational Science, UMR_S1148, INSERM, University Paris Diderot, France (M.J.-P.); and Department of Pediatrics, University of Colorado, Aurora (K.B.N.).

The online-only Data Supplement is available with this article at http://atvb.ahajournals.org/lookup/suppl/doi:10.1161/ATVBAHA.118.310731/-/DC1.

Correspondence to Keith B. Neeves, PhD, Chemical and Biological Engineering Department, Colorado School of Mines, 1500 Illinois St, Golden, CO 80401. E-mail kneeves@mines.edu

Nonstandard Abbreviations and Acronyms	
GPVI	glycoprotein VI
HCT	hematocrit
NPP	normal pooled plasma
PRP	platelet-rich plasma
RBC	red blood cells
Re	Reynolds number
TF	tissue factor
VT	venous thrombosis

The histology of venous thrombi implies a role for blood flow in thrombus propagation. The alternating layered structure of red, fibrin-rich regions that begin at the vessel wall in the valve sinus followed by white, platelet-rich regions suggests a mechanism of platelet accumulation to the initial fibrin-rich regions.[13] The geometry of the valve sinus defined by a large cavity distal to the expansion created by the valve leaflets yields unique flow patterns. Flow through fixed venous valves of dogs shows a large primary vortex adjacent to the valve cusps and a secondary vortex in the deepest recess of the valve pocket.[14] The fluid velocity in this secondary vortex is extremely slow and corresponds to the most hypoxic area of the valve sinus.[15] Vortical flows in the valve sinus have also been observed by ultrasound in human venous valves.[16]

Vortical flows caused by flow separation downstream of a stenosis or sudden expansion support thrombus formation.[17] Blood cells that enter these flows have a long residence time that promotes platelet–platelet collisions and ultimately aggregation in sudden annular expansions.[18] RBC enhance the accumulation of platelets in vortical flows in a hematocrit (HCT)-dependent manner.[15,18,19] The low wall shear rates in vortical flows support platelet adhesion to collagen and neutrophil adhesion to P-selectin, with the most accumulation occurring near reattachment points in sudden annular expansions and backwards facing steps.[18,20,21] These geometries are relevant to arterial thrombosis or vascular injuries where collagen is exposed to flowing blood; however, they do not incorporate TF-dependent coagulation or fibrin deposition, which are central to the pathophysiology of VT.

In this study, we present TF-initiated thrombus propagation in a model venous valve. We use scaling arguments to fabricate valve geometries that have geometric similarity to human valves. A sudden expansion geometry with undercuts of different angles results in primary and secondary vortices at sufficiently high flow rates. An initial fibrin-rich thrombus forms in the secondary vortex; however, RBC and platelets within the primary vortex are necessary to propagate the thrombus.

Materials and Methods

Materials

Materials are available in the online-only Data Supplement.

Computational Fluid Mechanics

Flow through the model venous valve was simulated at steady state for the 90°, 120°, 135°, and 150° angles using the same dimensions as the device using computational fluid dynamics software (COMSOL Multiphysics, COMSOL Inc, Burlington, MA). The entrance condition was set as a constant flow rate to match the Reynolds number, Re, for a Newtonian fluid with a viscosity of 3.5 cP. The outlet condition was set as a zero pressure. The other boundary conditions were set to no-slip. The solution to the Navier–Stokes equation was calculated at a finer mesh size (1 379 416 elements). The simulations were repeated at a fine (422 701 elements), normal (159 625 elements), and coarse (76 256 elements) mesh to insure grid independence (Figure I in the online-only Data Supplement).

Re Matching

The Re is a nondimensional number that compares viscous to inertial forces in flow. It is given by

$$\mathrm{Re} = \frac{\rho v D}{\mu},$$

where ρ is the fluid density, μ the fluid viscosity, v the average velocity, and D is the characteristic dimension (the channel height in our case). When we increased the HCT, we increased the viscosity of the suspension. At the same flow rate, this would lead to a smaller Re. To achieve dynamic similarity and match Re across different HCT, we estimate the viscosity using

$$\mu_{rel} = 1 + 2.86\left[(1-\mathrm{HCT})^{-0.769} - 1\right],$$

where μ_{rel} is the viscosity of the suspension relative to the suspending fluid viscosity, and HCT the hematocrit.[22] These flow rates are in Tables I and II in the online-only Data Supplement for plasma and buffer, respectively.

Microfluidic Devices

The flow chamber consists of 150 μm wide PDMS (polydimethylsiloxane) channels expanding into a 450-μm wide channels at angles 90°, 120°, 135°, or 150°, where larger angles represent a more severe undercut. A vacuum chamber surrounds the channels to aid in the removal of air bubbles. Fabrication details are found in the online-only Data Supplement.

Visualization of Streaklines

To measure streaklines, 3-μm fluorescein isothiocyanate–labeled polystyrene beads at a number density of 200 000/μL in HEPES-buffered saline (HBS) were mixed with washed RBC at HCT of 0, 0.2, 0.4, and 0.6. A 500-μL Hamilton Gastight syringe was filled with the suspension and connected to a microfludic device via 0.01″ ID tubing. Flows rates were set to match desired Re of 0.1, 10, and 25. Images were acquired with an inverted microscope (Olympus IX81, ×20 numerical aperture [NA]=0.45, excitation/emission [ex/em] 475/505 nm) at 100 ms exposure.

Blood Collection

All procedures followed were in accordance with the ethical standards of the responsible committee on human experimentation (University of Colorado, Boulder) and with the Helsinki Declaration of 1975, as revised in 2000. Informed consent was obtained from all subjects for being included in the study. Blood was collected from healthy donors by venipuncture into 4.5 mL vacutainer tubes containing 3.2% sodium citrate. The first tube of blood collected was treated as waste to eliminate any activated platelets because of venipuncture. Donors had not consumed alcohol within 48 hours before the draw nor had they taken any prescription or over-the-counter drugs within the previous 10 days excluding oral contraception.

Procedures for Platelet-Rich Plasma, Reconstituted Blood, and Plasma With RBC Suspensions

Platelet-rich plasma (PRP) and packed RBC were obtained by centrifugation of citrated whole blood at 200*g* for 20 minutes. The top fraction above the buffy coat was collected for PRP, and platelet counts were measured by flow cytometry (EMD Millipore, guava easyCyte 6 2L, Hayward, CA) gated by size. The bottom fraction contained packed RBC. Hematocrit of

the packed RBC was measured with a CritSpin (Beckman Coulter, Brea, CA) following the manufacturer's instructions. For experiments where RBC were added into PRP to give reconstituted blood, packed RBC and PRP were combined to achieve the desired hematocrit without wash steps (eg, if the assay was to be run at HCT 0.4, we prepared the blood at HCT 0.44 to account for the additional volume of the recalcification buffer). For experiments where RBC were added into normal pooled plasma (NPP), the RBC were first washed 3× with RBC buffer for 5 minutes at 2000*g*. NPP was added back to the RBCs to achieve the desired HCT concentrations. $DiOC_6$ (3,3′-dihexyloxacarbocyanine iodide; 1 µmol/L) and Alexa 555–labeled fibrinogen were added to each preparation (NPP, PRP, NPP+RBC, reconstituted blood) to a final concentration 28 µg/mL for 15 minutes at 37°C before introduction into the device.

Reconstituted Blood Rheology

Packed RBC (see above for centrifugation procedure) were added to autologous donor plasma or NPP to achieve an HCT of 0.4. The RBC suspension (17 mL) was introduced into the cup (diameter=30.02 mm; depth=78.01 mm) of the Peltier Concentric Cylinder system of the DH-3 rheometer, after which the bob (diameter=27.96 mm; depth=41.91 mm) was lowered into position with an operating gap of 5.91 mm, and temperature was maintained at 37°C. FC-40 oil (1 mL; viscosity=1.5 cSt) was carefully pipetted on top of the suspension to prevent aggregation at the air–liquid interface. The shear rate sweep from 0.1 to 1000/s was performed for 10 seconds at each shear rate to measure the shear-dependent viscosity of the RBC suspension blood. Measurements were taken every 5 minutes for 45 minutes in total. The viscosity of the autologous donor plasma and NPP were measured at 100/s to calculate the relative viscosity for each suspension.

Microfluidic Device Operation

Stock Innovin TF was diluted 1:9 in HBS and used to pattern the post-expansion half of the channel including the pockets by carefully backfilling via pipette aspiration. The device was connected to vacuum to ensure that there were no air bubbles in the valve pocket. After a 1-hour incubation of TF at room temperature, the small tubing, connector, and large tubing were connected as shown in Figure II in the online-only Data Supplement. A 60-mL syringe was filled with 2% BSA in HBS to the 25 mL mark, and a 3 mL syringe is filled with recalcification solution to the 3 mL mark. The 3 mL syringe is connected first to the calcium inlet, and recalcification buffer is perfused until it comes out of the blood inlet. Then the 60-mL syringe is connected. This order insures that the dead volume between the calcium inlet and the T-junction is filled with calcium buffer and not BSA solution. The syringes were placed onto a syringe pump (Harvard Apparatus PhD 2000), the flow rate set to match the desired Re (Table I in the online-only Data Supplement), and the solutions were perfused through the tubing for 5 minutes to insure a tight connection with the pump as well as to block the tubing along the path of blood flow. The tubing was then connected to the inlet of the microfluidic device, and an additional tubing (60 cm, 0.01″ tubing) containing HBS was connected to an outlet of the device. The whole system was perfused for 5 minutes and allowed to block with 2% BSA in HBS for an additional hour.

Reconstituted Blood Studies

When the plasma, RBC suspension, PRP, reconstituted blood, or whole blood was ready for perfusion, the 60-mL syringe was emptied of the blocking solution and filled with one of these solutions or suspensions to the same volume it held before removal to insure it will fit on the syringe pump without adjustments. Flow was started immediately. Images of the valve pocket were captured every 20 seconds in a confocal microscope (Olympus FV10i, ×60 objective NA=0.95) at 3 z-locations. Alternatively, for thrombus area assays, images were captured with an inverted microscope (Olympus IX81, ×20 NA=0.45, ex/em 475/505 nm, 545/580 nm) every 10 seconds.

Whole Blood and Platelet Inhibitor Studies

Citrated whole blood from one blood draw was separated into two 13 mL samples. The first sample was supplemented with vehicle control (HBS for the abxicimab, ACT017, and D-dimer, dimethyl sulfoxide for atopaxar) or the inhibitor (20 µg/mL abxicimab,[23] 500 nmol/L atopaxar,[24] 100 µg/mL ACT017,[25] 30 µg/mL D-dimer[26]). $DiOC_6$ (1 µmol/L) and Alexa 555–labeled fibrinogen (final concentration, 28 µg/mL) were added to the preparation for 15 minutes at 37°C. The sample was then perfused as in the reconstituted blood case (HCT, 0.4) at 372 µL/min through the device for 30 minutes. The second sample was then loaded with the drug or vehicle control and labeled for 15 minutes at 37°C and perfused through a second device under the same conditions. Images were captured with an inverted microscope (Olympus IX81, ×10 NA=0.3, ex/em 475/505 nm, 545/580 nm) every 10 seconds.

Phophatidylserine Labeling

Assays were run with reconstituted whole blood (HCT, 0.4) at Re=10. After 25 minutes of perfusion, flow was stopped, and the channel was rinsed 3× with Annexin V–binding buffer in the same direction of flow (blood inlet to blood outlet) using a pipette. The clot was then fixed by filling the channel with 2% glutaraldehyde in HBS for 10 minutes. The channel was then rinsed with the Annexin V–binding buffer and then filled with the Annexin V label mixed 1:1 with the binding buffer. The sample was incubated in the dark at room temperature for 45 minutes and then rinsed with Annexin V–binding buffer and imaged by confocal microscopy.

Image Quantification

Thrombus areas were measured by thresholding the overlay of platelet and fibrin(ogen) images using ImageJ (National Institutes of Health, Bethesda, MD). Integrated fluorescence of platelet accumulation was measured using ImageJ, and the average grayscale pixel brightness normalized by the maximum (4096 for a 16-bit TIFF).

Statistical Analysis

Data were determined normally distributed by the Anderson–Darling test. Statistical differences were measured using a Student *t* test or Mann–Whitney *U* test (for data sets that failed the Anderson–Darling test) for pairs and 1-way ANOVA for groups followed by a post hoc Tukey honestly significant difference procedure to compare pairs in MATLAB (R2016b, MathWorks, Natick, MA).

Results

Design and Characterization of Model Venous Valves

The flow through human venous valves depends on vessel size and body position. For example, in the common femoral vein, mean peak velocities ranged from 37.3 cm/s in supine leg up position to 1.3 cm/s in a sitting position.[27] At this scale, a prohibitive volume of blood would be required for observing thrombus formation in a single pass device. Therefore, we used a scaling approach to develop a model vein and venous valve with dimensional similarity to human venous valves.[28] The vessel stenosis ratio—vessel diameter:distance between valve leaflets—is the primary geometric ratio that dictates flow in an expansion. This ratio is ≈3:1 in the human greater saphenous vein and superficial femoral vein.[16,29] In the scaled model, we use a 450-µm wide channel as the vessel and a 150-µm wide channel as the stenosis to achieve a 3:1 stenosis ratio. Previous studies have examined hemodynamics in a sudden expansion or stenosis to model arteriosclerotic geometries[30,31]; however, the existence of a valve sinus distal to the expansion created by the valve leaflets likely influences the flow field in large veins. To model the valve sinus, we fabricated devices with undercut angles of 90°, 120°, 135°, or 150° (Figure 1A).

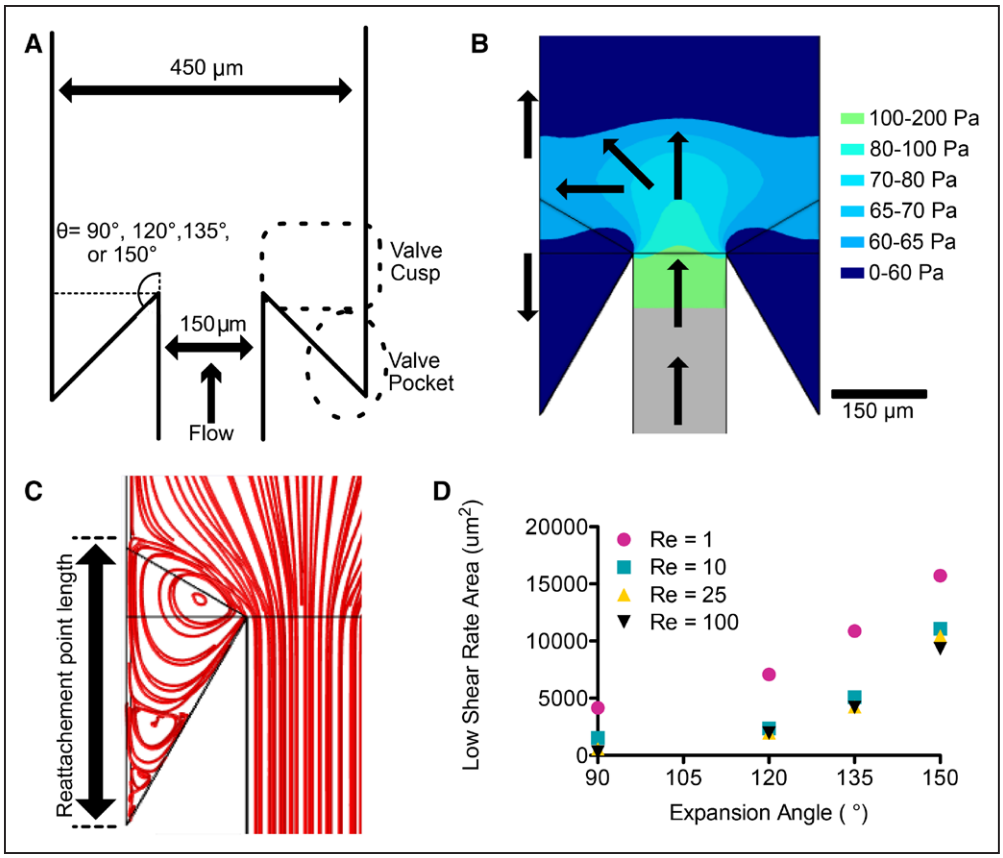

Figure 1. A, Geometry of the model venous valve. The device consists of an expansion from 150-µm wide channel to 450-µm wide channel with a height of 141 µm. The angle of expansion was 90°, 120°, 135°, or 150°. The zone behind the expansion is designated the valve cusp. The deeper part of the sinus is designated as the valve pocket. **B**, Visualization of the gauge pressure after a 150° expansion for a Reynolds number (Re) of 10. The pressure in the valve sinus is lower than the downstream pressure, resulting in a reversed flow. The arrows roughly depict average flow directions. **C**, Streamlines for the 150° expansion for Re of 10. The flow reattachment point distance is measured from the corner to the end of the primary vortex. **D**, The area with a wall shear rate of <50/s as calculated by the simulation for Re of 1, 10, 25, and 100 and the expansion angles of 90°, 120°, 135°, or 150°.

We refer to the area near the opening of the valve sinus, the valve cusp, and the deeper regions as the valve pocket. The Re in veins can vary from 1 to 600 although in large human veins is typically Re >100.[27,32,33] The Re is a dimensionless quantity that characterizes the relative importance of inertial forces to viscous forces. To avoid shear-induced platelet activation,[34] we limited ourselves to Re=1 to 25, which is comparable to reports in fixed canine valves.[14] In flows with Re >1, inertial forces dominate. For sufficiently high Re, flow separation arises because of a counter acting pressure gradient against the direction of flow immediately downstream of the sudden expansion (Figure 1B). Fluid far from the wall has more inertia and is able to overcome this pressure gradient and continue downstream, but viscous forces acting on fluid in the near wall region reduce the inertia so that it cannot overcome the pressure gradient, causing recirculation. This flow separation is characterized by detachment and reattachment points (Figure 1C), as well as regions of low wall shear rates that are favorable for fibrin deposition. The area of the valve pocket with a wall shear rate <50/s, which can support fibrin deposition in the absence of blood cells,[35] depends on the Re and, more strongly, the undercut angle as predicted by simulations (Figure 1D). Above Re of 10, which is characteristic of large veins,[29] the low shear rate area was independent of Re. This suggests that valve geometry, more than blood flow, dictates flow in the valve pocket.

To visualize the flow field in the absence of blood cells, we perfused suspensions of 3 µm fluorescent particles through the scaled model and measured their streaklines (Figure 2A). At Re=1 and all angles, we observe a particle free region in the valve pocket as indicated by the dark zones where few fluorescent particles were observed over a 1-hour experiment. Those particles that entered the corners of these zones had little apparent convective velocity, suggesting no or a small circulating flow. At Re=10, we observed flow separation and the entrainment of particles in a primary vortex at undercut angles of 135° and 150° as indicated by particle streaklines that move countercurrent to the bulk flow. At Re=25, we observed particle accumulation in the primary vortex at all angles except for 90°. The reattachment length as defined in Figure 1C increased with increasing Re (Figure III in the online-only Data Supplement). For a given Re, increasing the angle also increases the reattachment length (Figure III in the online-only Data Supplement). At angles of 135° and 150°, particles were also observed in a secondary vortex for Re of 10 and 25, which was designated by slow moving particles in the valve pocket (Movie I in the online-only Data Supplement).

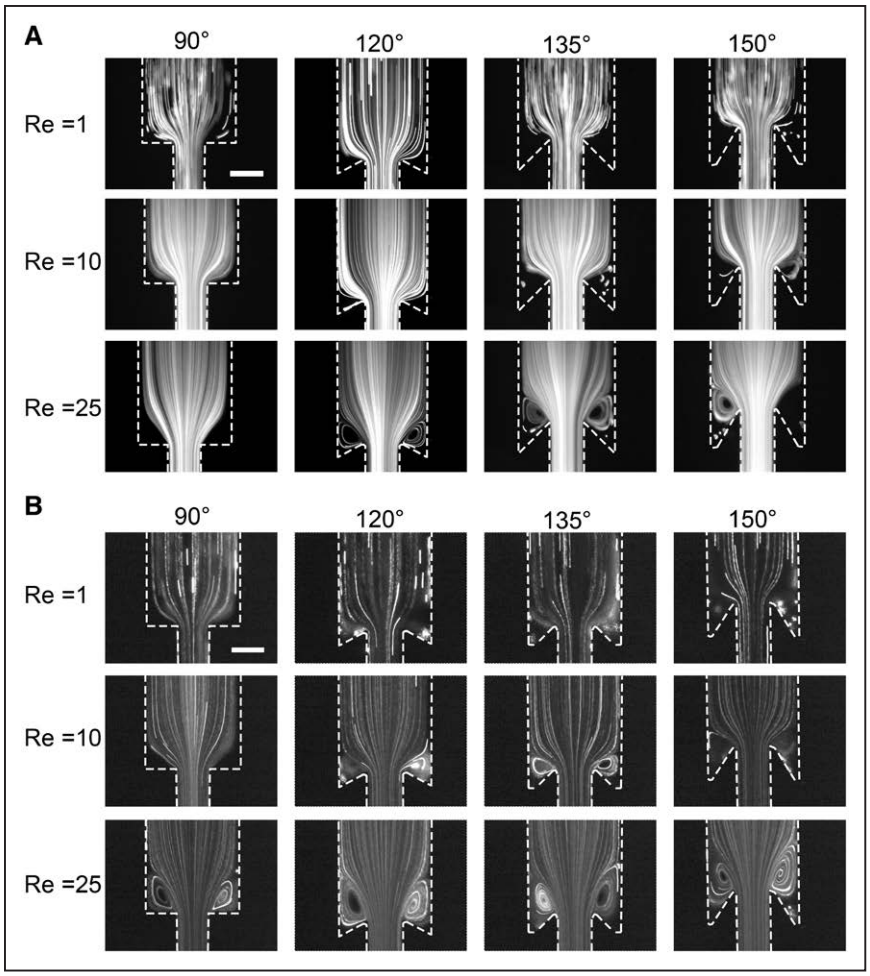

Figure 2. Visualization of the flow field in model venous valves. **A**, Perfusion of 3 μm fluorescent beads in buffer through the device for the 90°, 120°, 135°, and 150° expansion at Reynolds number (Re) of 1, 10, and 25. **B**, Perfusion of 3 μm fluorescent beads at HCT (hematocrit) 0.2 in buffer through the device for the 90°, 120°, 135°, and 150° expansion at Re of 1, 10, and 25. The primary vortex grows as a function of Re at both angles. The low flow, cell-poor region (valve pocket) is visible at higher undercut angles, and more beads enter the vortices in the presence of red blood cell. Scale bar, 200 μm.

RBC Enrich the Valve Pocket With Platelets and Platelet Sized Particles

In the presence of RBC, we observed enhanced entrainment of fluorescent particles in the valve pocket for HCT of 0.2, 0.4, and 0.6 compared with experiments with no RBC (Figure 2B; Figure IV and Video I in the online-only Data Supplement). To provide a faithful comparison of the flow field independent of HCT, the Re rather than the flow rate were matched. An HCT-dependent function for the viscosity was used to calculate Re (see Methods).[22] The reattachment length remained constant across matched Re for all HCT values, confirming that this is the appropriate scaling parameter (Figure III in the online-only Data Supplement). In experiments where TF was immobilized in the valve pocket, the rate of platelet accumulation in the valve pocket was enhanced by ≈3-fold in reconstituted blood with an HCT of 0.4 compared with PRP (P=0.0213; Figure V in the online-only Data Supplement). In the 135° and 150° expansion angles, RBC also entered and became trapped in the valve pocket and the initial fibrin gel (Movie II in the online-only Data Supplement). These data show that RBC enhance the transport of platelet and platelet sized particles into the valve pocket.

Low Flow Regions in Model Valve Pockets Support Initial Fibrin Formation and Thrombus Growth

To determine the influence of undercut angle on the initiation of thrombus formation, PRP and reconstituted blood (PRP with RBC) were perfused at a Re of 10 through devices with undercut angles of 90° and 150°, where TF was immobilized on the surface of the model valve sinus (Figure 3A; Movies III and IV in the online-only Data Supplement). Fibrin deposition occurred in the lowest flow regions within 10 minutes for the 90° undercut angle and within 5 minutes for the 150° undercut angle. Initial fibrin deposition coincided with areas with a wall shear rate of <50/s (Figure 3B). For a 90° undercut angle, simulations predict a single vortex (Figure 3C), and only moderate fibrin formation was observed followed by platelet accumulation (Figure 3A). For a 150° undercut angle, a fibrin gel first fills the area coinciding with the predicted secondary vortex (Figure 3C), followed by platelet adhesion and aggregation which then support spatial propagation of the thrombus that ultimately grows out of the valve pocket (Figure 3A). These data suggest that the valve pocket geometry and in particular regions of very low flow protect coagulation and fibrin polymerization reactions and support initial platelet accumulation.

Platelets and RBC Are Necessary for Thrombus Propagation Out of the Valve Sinus

To determine the roles of platelets and RBC on thrombus growth in our model valve sinus, NPP, PRP, NPP containing RBC, and reconstituted blood (PRP with RBC) were perfused at an Re of 10 through devices with a 150° undercut angle (Figure 4A).

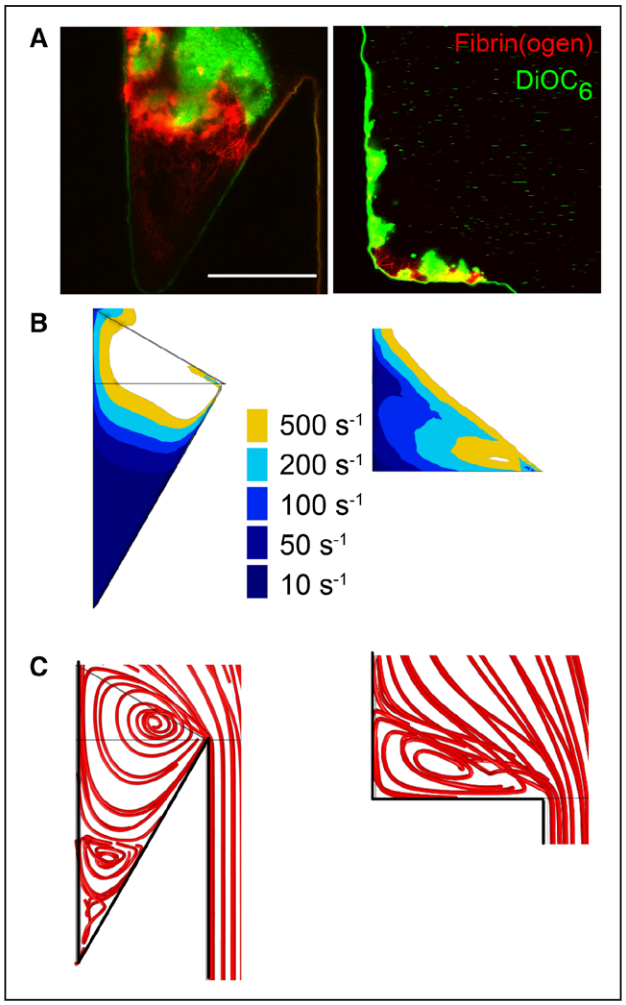

Figure 3. The effect of undercut angle on thrombus formation and the flow field. **A**, Thrombus formation in the 150° (**left**) and 90° (**right**) undercut angle for reconstituted blood (HCT [hematocrit]=0.4) after 15 min in tissue factor–coated device at Reynolds number (Re)=10. Platelets are shown in green, and fibrin(ogen) is shown in red. Scale bar, 150 μm. Wall shear rate contours (**B**) and streamlines (**C**) from simulations for undercut angles of 150° (**left**) and 90° (**right**) at Re=10.

For NPP, fibrin formed within 3 to 5 minutes in the valve pocket region with the lowest shear rate as described above but did not extend beyond the area defined by the initial secondary vortex (Figure 4A; Movie IV in the online-only Data Supplement). Note the concave interface of the fibrin gel mirrors the interface between the primary and secondary vortex from particle streaklines (Figure 2) and simulations (Figure 3). Fibrin fibers were densest at the interface, suggesting an accumulation of coagulation proteins and fibrin(ogen) transported by flow into the primary vortex. The interface moved slowly; it extended just 50 μm over 30 minutes. Control experiments in the absence of immobilized TF showed fibrin deposition only in the deepest part of the valve pocket and only after 30 minutes of perfusion (Video V in the online-only Data Supplement).

PRP yielded similar sized thrombi as NPP (Figure 4A; Movie IV in the online-only Data Supplement). Platelets tend to accumulate near the detachment point at the valve cusp and to a lesser extent at the fibrin gel interface within the primary vortex. In regions near adhered platelets, the fibrin gel grows denser with time relative to gels formed with NPP, possibly because of platelet retraction or additional coagulation. However, thrombus size is similar to that of NPP after 30 minutes (Figure 4B). Thus, platelets in the absence of RBC do not support the propagation of thrombi beyond the low flow region defined by the secondary vortex.

NPP with suspended RBC at HCT of 0.4 and 0.6 yielded fibrin deposition that was also limited to the valve pocket. Here, the morphology of the fibrin gel is different because RBC were incorporated in the fibrin gel (Figure 4A). However, these RBC did not support additional thrombus growth beyond what was observed for NPP after 30 minutes (Figure 4B; Movie IV in the online-only Data Supplement). In control experiments without TF, RBC became trapped in the valve pocket, but no fibrin fibers were observed (Movie V in the online-only Data Supplement). It does not seem that RBC alone support additional coagulation that results in observable enhancement of thrombus growth compared with plasma alone. The shear-dependent viscosity of RBC suspended in NPP or autologous plasma was statistically similar (Figure VI in the online-only Data Supplement), suggesting that RBC agglutination was not enhanced in NPP.

Reconstituted blood containing both platelets and RBC supports robust thrombus growth out of the valve pocket and into the bulk flow. These thrombi were roughly double the size of those formed with NPP, PRP, and NPP with RBC at 30 minutes (Figure 4B; Movie IV in the online-only Data Supplement). Compared with PRP, experiments with reconstituted blood show that platelets in the primary vortex adhere in a dense layer to the initial fibrin gel formed in the valve pocket, followed by the rapid formation of a thrombus that extends past the primary vortex (Figure 4A; Movie IV in the online-only Data Supplement). The thrombi grew beyond the field-of-view during some experiments, so exact thrombus sizes were not available for all assays. HCT of 0.4 and 0.6 yielded similar thrombus growth rates and sizes (Figure 4B). Alternating platelet- and RBC-rich zones are apparent as the thrombus penetrated into the main channel (Movies II and IV in the online-only Data Supplement).

Reconstituted blood (RBC, platelets, and plasma) and whole blood yield similar results in terms of thrombus area and growth rate (Figure VII in the online-only Data Supplement). These data suggest that leukocytes do not play a significant role in this model of thrombus propagation.

Platelets Adhered to Fibrin in the Valve Sinus Can Become Procoagulant

In both PRP and reconstituted blood experiments, we observed regions in the valve pocket where the $DiOC_6$ dye, which labels the mitochondrial membrane, began to fade at around 10 minutes after initial adhesion (Figure 5A and 5B; Movie IV in the online-only Data Supplement). We hypothesized that this was indicative of mitochondrial depolarization because of platelet activation and would lead to subsequent exposure to phosphatidylserine.[33] To test this hypothesis, we performed

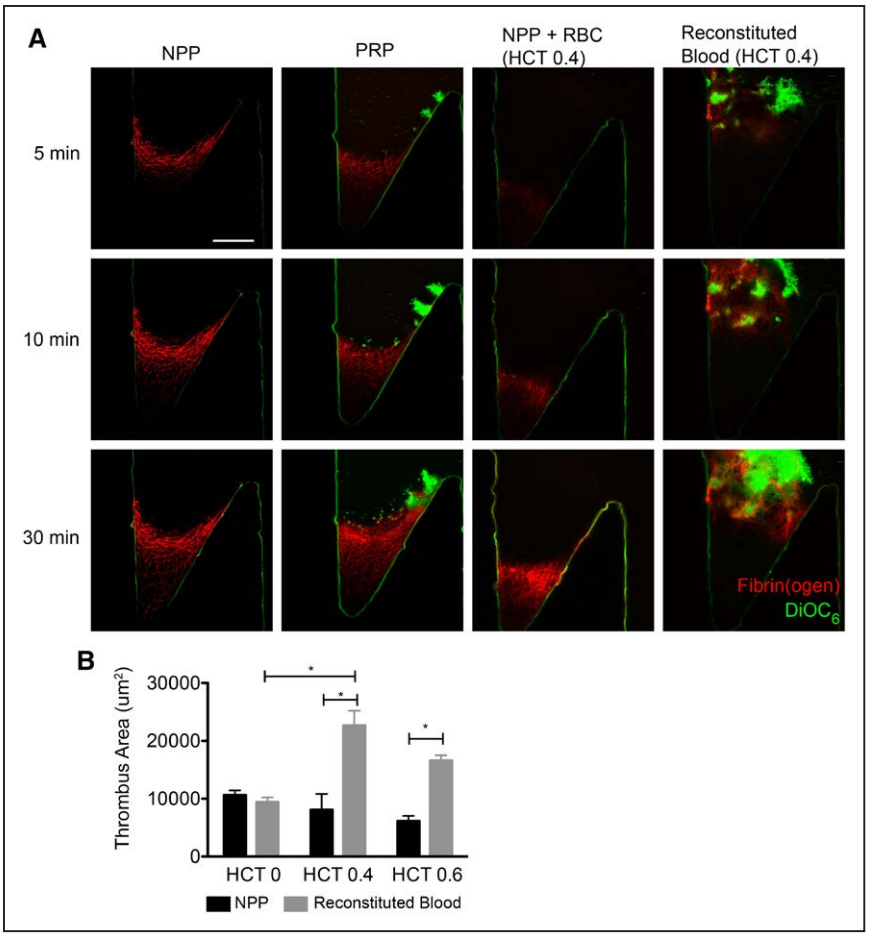

Figure 4. The role of platelets and red blood cells (RBC) on thrombus propagation. **A**, Normal pooled plasma (NPP), platelet-rich plasma (PRP), washed RBC in NPP (NPP+RBC, hematocrit [HCT]=0.4), and reconstituted whole blood (HCT=0.4) were perfused at Reynolds number=10 through the device. NPP, PRP, and RBC+NPP show a slow moving fibrin front that corresponds to the edge of the primary vortex and the transition to the valve pocket. For the reconstituted whole blood, RBC fill the valve pocket, diminishing the fluorescence signal of the fibrin(ogen). Focal plane 10 μm from the bottom surface. Platelets are shown in green ($DiOC_6$ [3,3′-dihexyloxacarbocyanine iodide]), and fibrin(ogen) is shown in red. Scale bar, 100 μm. **B**, The area of the thrombus was measured at 30 min for RBC in NPP at (black bars) and reconstituted blood (gray bars) for HCT of 0, 0.4, and 0.6 (n=5). The means and standard error are plotted. Statistical differences were measured by ANOVA followed by Tukey test for multiple comparisons.

experiments with reconstituted blood (HCT, 0.4) at Re of 10 for 25 minutes, fixed the thrombi, and then used annexin V to label phosphatidylserine (Figure 5C). We found that annexin V–positive platelets were localized in dense fibrin networks near the fluid-thrombus interface and in large platelet aggregates. Platelets that lost their $DiOC_6$ signal during the perfusion experiment were found to be annexin V positive after fixation.

Platelets Aggregation in the Valve Sinus Is Supported by GPVI Signaling

Finally, to determine what interactions mediate activation of platelets adhered to fibrin, we conducted experiments with a series of platelet receptor inhibitors. Whole blood was treated with the $\alpha_{IIb}\beta_3$ inhibitor abciximab, the PAR1 (protease-activated receptor 1) inhibitor atopaxar, an anti–glycoprotein VI (GPVI) humanized Fab fragment ACT017,[36] or D-dimer that binds to GPVI.[26,37] Blood was perfused at Re=10 through TF-coated devices with a 150° undercut angle. In all cases, an initial fibrin gel was formed as in reconstituted blood and plasma conditions. Abciximab abrogates platelet buildup beyond the first layer of platelets on the fibrin gel (Figure 6). Atopaxar, a PAR1 inhibitor, showed modest but not significant differences in thrombus area compared with vehicle controls. Treatment with ACT017 and D-dimer did reduce total thrombus area in a spatially dependent manner; platelets still aggregate around the corner proximal to the expansion, but their accumulation adjacent to fibrin in the valve pocket or on the distal wall was diminished.

Discussion

In this study, we designed a model of TF-initiated VT that captures some of the important hemodynamic features of human venous valves, specifically, primary and secondary vortices and flow separation in an expansion geometry with an undercut. An initial fibrin gel formed in the low flow region of the secondary vortex in the deepest part of the valve pocket independent of blood cells. Both RBC and platelets were necessary for thrombus growth beyond the valve pocket. Platelets support thrombus growth beyond the initial fibrin gel by adhering, activating, and for at least a subpopulation, becoming procoagulant. These results suggest a biophysical mechanism of thrombus propagation that depends on both flow-enhanced platelet–RBC interactions upstream of a valve and low flow niches that protect coagulation reactions and support platelet adhesion to fibrin (Figure VIII in the online-only Data Supplement).

The initiation of coagulation and fibrin polymerization require protection from dilution by blood flow.[38] Computational models of VT suggest that a threshold concentration of TF must first accumulate on the valve wall before coagulation can initiate.[39] Here, we have skipped the steps leading up the accumulation of TF and started with a surface TF concentration capable of initiating coagulation. Previous

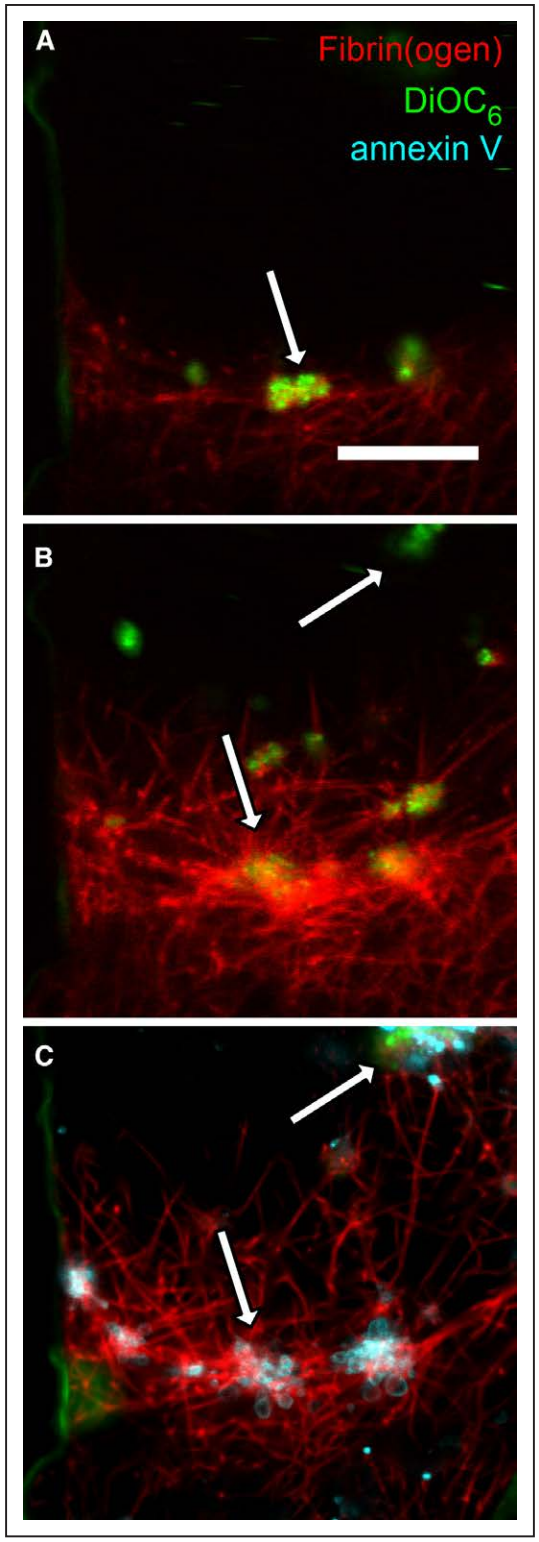

Figure 5. Fibrin adhered platelets become procoagulant. **A**, Initial platelet (green) deposition on fibrin fibers (red) in the valve pocket after reconstituted blood (HCT [hematocrit]=0.4) perfused at a Reynolds number of 10 for 5 min in a device with an undercut angle of 150°. **B**,The same field-of-view as (**A**) at 20 min. The platelet aggregate denoted by the arrow in (**A**) became a site for fibrin deposition. **C**, The same field-of-view as (**A**) after a 25 min perfusion and staining with annexin V (cyan). Annexin V localized on the edges of platelet aggregates and in the fibrin network as denoted by arrows. Scale bar, 20 μm.

studies found that even at high thrombin or TF concentrations, fibrin can only form at wall shear rates <100/s in the absence of adhered blood cells.[6,35] That is consistent with observations in this study, where the low flow region defined by shear rates of <50/s in the valve pocket was the nidus for fibrin deposition. The size of this initial fibrin gel was dictated by the degree of undercut, more so than the Re.

RBC promote thrombus propagation by enhancing the transport of platelets into the valve pocket at a sufficient rate to support coagulation beyond the TF-coated valve. Based on studies in nonbiological dense suspensions in sudden expansions where margination occurs because of size exclusion effects,[40] we would expect this is because of platelet margination upstream from the expansion point, rather than increased collision frequency within the vortices. Elevated hematocrit is correlated with increased risk for VT.[41] In our model, we did not observe a significant difference in thrombus growth between hematocrits of 0.4 and 0.6. However, these experiments were conducted at a constant Re to provide faithful comparison of the hemodynamics while the cardiovascular system is likely regulated by other parameters like oxygen demand.

The procoagulant activity of RBC reported by others[42] was not sufficient in these studies to initiate fibrin deposition in the absence of TF nor to enhance it in absence of platelets. This observation is consistent with in vivo, in vitro, and in silico models of arterial thrombosis where the primary influence of an elevated hematocrit is to promote platelet-dependent thrombus growth rather than coagulation.[43] RBC do contribute to the architecture and mechanics of venous thrombi; they are retained in fibrin-rich thrombi via factor XIII–dependent fibrin α-chain cross-linking[44,45] and organize to form densely packed structures following platelet-mediated contraction[46] that could limit transport of coagulation products into and out of the growing thrombus. RBC can also adhere to activated platelets and fibrin at low shear rates, such as those found in vortices.[47]

Platelet adhesion to fibrin and subsequent activation through GPVI are essential in this model for thrombus propagation. Platelets adhered to fibrin along the entire periphery of the primary vortex and formed a platelet-rich layer reminiscent of the laminate structure of thrombi formed in the venous valves of humans.[13] Some platelets within this layer become procoagulant, supporting the formation of an adjacent fibrin-rich thrombus that penetrates from the valve sinus into the bulk flow. In agreement with previous studies,[48,49] some platelets adhered to fibrin exposed phosphatidylserine. Treatments with the GPVI blocking Fab fragment (ACT017) or D-dimer reduced thrombus growth. This is consistent with reports that GPVI can bind to the D-domain on fibrin(ogen) although whether the monomer or dimer of GPVI governs this interaction is a subject of debate.[26,37] Importantly, D-dimer may also limit thrombus growth by inhibiting fibrin polymerization and $\alpha_{IIb}\beta_3$ interactions. Even when inhibiting GPVI, there was platelet accumulation around the corner that defines the valve cusp. Platelet accumulation in this region is possibly driven by activation-independent aggregation as previously shown downstream of stenotic geometries.[4]

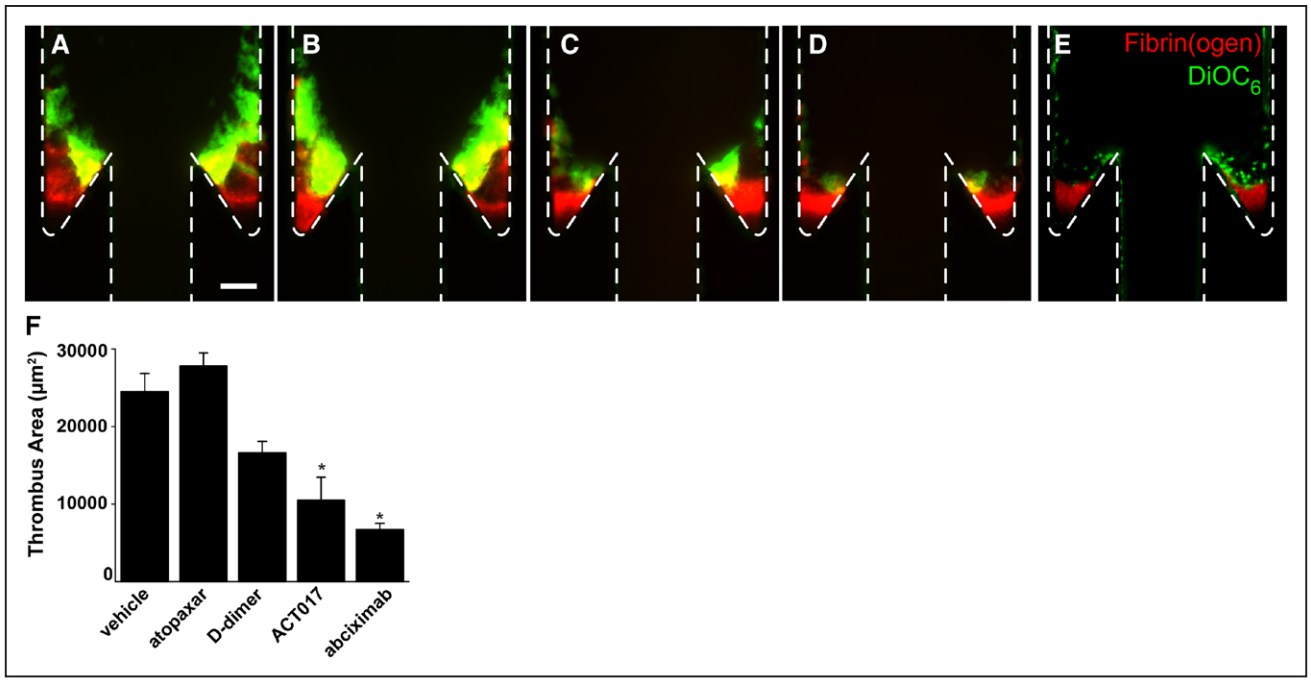

Figure 6. Thrombus growth is driven by platelet activation through glycoprotein VI (GPVI). Representative images of thrombus formation with whole blood for vehicle control (**A**) and treatments with atopaxar (**B**), D-dimer (**C**), anti-GPVI antibody ACT017 (**D**), and abciximab (**E**) after 30-min perfusion. Scale bar, 100 μm. **F**, Thrombus areas for vehicle controls and each treatment. The means (n=6) and standard error are plotted. Statistical differences between vehicle and inhibitors were measured by ANOVA followed by Tukey test for multiple comparisons.

There is not an established relationship between GPVI and VT risk in humans. However, reduced platelet responsiveness to GPVI agonists, which is presumed to be a consequence of continuous activation, is associated with a higher risk of venous thromboembolism.[50] Our findings that platelets are necessary for thrombus propagation in an in vitro model using human blood are consistent with the murine IVC flow restriction model.[11] In our model, platelets do not play a significant role in the initiation of a thrombus, which is consistent with a lack of platelets at the thrombus nidus in vivo (the valve pocket in our model), but presence in successive layers (the valve cusp and beyond).[51] In some animal models of VT, platelets play an essential role in early events thrombus growth[11,52] although it is difficult to delineate initiation from propagation in these models.

There are several limitations of this study. First, because the model valve leaflet is fixed, we do not capture the hemodynamics associated with valve opening and closing. This is an approach similar to other in vitro and computational studies of VT,[12,39] and we argue it is a relevant model for valvular stasis. Second, to use a nonprohibitive volume of human blood and avoid shear-induced platelet activation, we used scaling arguments to create a small version of a human venous valve. This model captures the essential hemodynamics, but the time scale for thrombus propagation is naturally shortened because of the smaller length scales. Third, leukocytes and specifically neutrophils and neutrophil extracellular traps may play a role in the initiation of VT.[11,52,53] These mechanisms were not explicitly studied here; however, the presence of leukocytes in whole-blood experiments did not seem to influence thrombus growth or size compared with reconstituted blood without leukocytes. Fourth, the surface-bound anticoagulants thrombomodulin and heparin sulfate are not present in this model. Computational studies suggest that coagulation can be initiated in the presence of these anticoagulants with a sufficient quantity of TF.[12,54]

Acknowledgments

We thank Anticor Biotech for the kind gift of the anti–glycoprotein VI Fab ACT017.

Sources of Funding

This work was supported by the National Science Foundation CAREER (CBET-1351672), American Heart Association (14GRNT20410094), and the National Institutes of Health (R01HL120728).

Disclosures

None.

References

1. Versteeg HH, Heemskerk JW, Levi M, Reitsma PH. New fundamentals in hemostasis. *Physiol Rev*. 2013;93:327–358. doi: 10.1152/physrev.00016.2011.
2. Mackman N. Mouse models, risk factors, and treatments of venous thrombosis. *Arterioscler Thromb Vasc Biol*. 2012;32:554–555. doi: 10.1161/ATVBAHA.112.246173.
3. Singh I, Smith A, Vanzieleghem B, Collen D, Burnand K, Saint-Remy JM, Jacquemin M. Antithrombotic effects of controlled inhibition of factor VIII with a partially inhibitory human monoclonal antibody in a murine vena cava thrombosis model. *Blood*. 2002;99:3235–3240.
4. Nesbitt WS, Westein E, Tovar-Lopez FJ, Tolouei E, Mitchell A, Fu J, Carberry J, Fouras A, Jackson SP. A shear gradient-dependent platelet aggregation mechanism drives thrombus formation. *Nat Med*. 2009;15:665–673. doi: 10.1038/nm.1955.
5. Sakariassen KS, Aarts PA, de Groot PG, Houdijk WP, Sixma JJ. A perfusion chamber developed to investigate platelet interaction in flowing blood

with human vessel wall cells, their extracellular matrix, and purified components. *J Lab Clin Med*. 1983;102:522–535.
6. Onasoga-Jarvis AA, Puls TJ, O'Brien SK, Kuang L, Liang HJ, Neeves KB. Thrombin generation and fibrin formation under flow on biomimetic tissue factor-rich surfaces. *J Thromb Haemost*. 2014;12:373–382. doi: 10.1111/jth.12491.
7. Mackman N. New insights into the mechanisms of venous thrombosis. *J Clin Invest*. 2012;122:2331–2336. doi: 10.1172/JCI60229.
8. Malone PC, Agutter PS. Deep venous thrombosis: the valve cusp hypoxia thesis and its incompatibility with modern orthodoxy. *Med Hypotheses*. 2016;86:60–66. doi: 10.1016/j.mehy.2015.12.002.
9. Chiu JJ, Chien S. Effects of disturbed flow on vascular endothelium: pathophysiological basis and clinical perspectives. *Physiol Rev*. 2011;91:327–387. doi: 10.1152/physrev.00047.2009.
10. Bovill EG, van der Vliet A. Venous valvular stasis-associated hypoxia and thrombosis: what is the link? *Annu Rev Physiol*. 2011;73:527–545. doi: 10.1146/annurev-physiol-012110-142305.
11. von Brühl ML, Stark K, Steinhart A, et al. Monocytes, neutrophils, and platelets cooperate to initiate and propagate venous thrombosis in mice in vivo. *J Exp Med*. 2012;209:819–835. doi: 10.1084/jem.20112322.
12. Elizondo P, Fogelson AL. A mathematical model of venous thrombosis initiation. *Biophys J*. 2016;111:2722–2734. doi: 10.1016/j.bpj.2016.10.030.
13. Sevitt S. The structure and growth of valve-pocket thrombi in femoral veins. *J Clin Pathol*. 1974;27:517–528.
14. Karino T, Motomiya M. Flow through a venous valve and its implication for thrombus formation. *Thromb Res*. 1984;36:245–257.
15. Jordan A, David T, Homer-Vanniasinkam S, Graham A, Walker P. The effects of margination and red cell augmented platelet diffusivity on platelet adhesion in complex flow. *Biorheology*. 2004;41:641–653.
16. Lurie F, Kistner RL, Eklof B, Kessler D. Mechanism of venous valve closure and role of the valve in circulation: a new concept. *J Vasc Surg*. 2003;38:955–961. doi: 10.1016/S0741.
17. Karino T, Goldsmith HL, Motomiya M, Mabuchi S, Sohara Y. Flow patterns in vessels of simple and complex geometries. *Ann N Y Acad Sci*. 1987;516:422–441.
18. Karino T, Goldsmith HL. Aggregation of human platelets in an annular vortex distal to a tubular expansion. *Microvasc Res*. 1979;17(3 pt 1):217–237.
19. Zhao R, Marhefka JN, Shu F, Hund SJ, Kameneva MV, Antaki JF. Microflow visualization of red blood cell-enhanced platelet concentration at sudden expansion. *Ann Biomed Eng*. 2008;36:1130–1141. doi: 10.1007/s10439-008-9494-z.
20. Skilbeck C, Westwood SM, Walker PG, David T, Nash GB. Population of the vessel wall by leukocytes binding to P-selectin in a model of disturbed arterial flow. *Arterioscler Thromb Vasc Biol*. 2001;21:1294–1300.
21. Skilbeck C, Westwood SM, Walker PG, David T, Nash GB. Dependence of adhesive behavior of neutrophils on local fluid dynamics in a region with recirculating flow. *Biorheology*. 2001;38:213–227.
22. Pries AR, Neuhaus D, Gaehtgens P. Blood viscosity in tube flow: dependence on diameter and hematocrit. *Am J Physiol*. 1992;263(6 pt 2):H1770–H1778. doi: 10.1152/ajpheart.1992.263.6.H1770.
23. Maxwell MJ, Westein E, Nesbitt WS, Giuliano S, Dopheide SM, Jackson SP. Identification of a 2-stage platelet aggregation process mediating shear-dependent thrombus formation. *Blood*. 2007;109:566–576. doi: 10.1182/blood-2006-07-028282.
24. French SL, Arthur JF, Lee H, Nesbitt WS, Andrews RK, Gardiner EE, Hamilton JR. Inhibition of protease-activated receptor 4 impairs platelet procoagulant activity during thrombus formation in human blood. *J Thromb Haemost*. 2016;14:1642–1654. doi: 10.1111/jth.13293.
25. Mangin PH, Tang C, Bourdon C, Loyau S, Freund M, Hechler B, Gachet C, Jandrot-Perrus M. A humanized glycoprotein VI (GPVI) mouse model to assess the antithrombotic efficacies of anti-GPVI agents. *J Pharmacol Exp Ther*. 2012;341:156–163. doi: 10.1124/jpet.111.189050.
26. Onselaer MB, Hardy AT, Wilson C, Sanchez X, Babar AK, Miller JLC, Watson CN, Watson SK, Bonna A, Philippou H, Herr AB, Mezzano D, Ariëns RAS, Watson SP. Fibrin and D-dimer bind to monomeric GPVI. *Blood Adv*. 2017;1:1495–1504. doi: 10.1182/bloodadvances.2017007732.
27. Ashby EC, Ashford NS, Campbell MJ. Posture, blood velocity in common femoral vein, and prophylaxis of venous thromboembolism. *Lancet*. 1995;345:419–421.
28. McCarty OJ, Ku D, Sugimoto M, King MR, Cosemans JM, Neeves KB; Subcommittee on Biorheology. Dimensional analysis and scaling relevant to flow models of thrombus formation: communication from the SSC of the ISTH. *J Thromb Haemost*. 2016;14:619–622. doi: 10.1111/jth.13241.
29. Nam KH, Yeom E, Ha H, Lee SJ. Velocity field measurements of valvular blood flow in a human superficial vein using high-frequency ultrasound speckle image velocimetry. *Int J Cardiovasc Imaging*. 2012;28:69–77. doi: 10.1007/s10554-010-9778-x.
30. Karino T, Goldsmith HL. Flow behaviour of blood cells and rigid spheres in an annular vortex. *Philos Trans R Soc Lond B Biol Sci*. 1977;279:413–445.
31. Wootton DM, Ku DN. Fluid mechanics of vascular systems, diseases, and thrombosis. *Annu Rev Biomed Eng*. 1999;1:299–329. doi: 10.1146/annurev.bioeng.1.1.299.
32. Ku DN, Klafta JM, Gewertz BL, Zarins CK. The contribution of valves to saphenous vein graft resistance. *J Vasc Surg*. 1987;6:274–279.
33. Helps EP, Mcdonald DA. Observations on laminar flow in veins. *J Physiol*. 1954;124:631–639.
34. Kroll MH, Hellums JD, McIntire LV, Schafer AI, Moake JL. Platelets and shear stress. *Blood*. 1996;88:1525–1541.
35. Neeves KB, Illing DA, Diamond SL. Thrombin flux and wall shear rate regulate fibrin fiber deposition state during polymerization under flow. *Biophys J*. 2010;98:1344–1352. doi: 10.1016/j.bpj.2009.12.4275.
36. Lebozec K, Jandrot-Perrus M, Avenard G, Favre-Bulle O, Billiald P. Design, development and characterization of ACT017, a humanized Fab that blocks platelet's glycoprotein VI function without causing bleeding risks. *MAbs*. 2017;9:945–958. doi: 10.1080/19420862.2017.1336592.
37. Induruwa I, Moroi M, Bonna A, Malcor JD, Howes JM, Warburton EA, Farndale RW, Jung SM. Platelet collagen receptor GPVI-dimer recognizes fibrinogen and fibrin through their D-domains, contributing to platelet adhesion and activation during thrombus formation. *J Thromb Haemost*. 2018;16:389–404. doi: 10.1111/jth.13919.
38. Rana K, Neeves KB. Blood flow and mass transfer regulation of coagulation. *Blood Rev*. 2016;30:357–368. doi: 10.1016/j.blre.2016.04.004.
39. Dydek EV, Chaikof EL. Simulated thrombin responses in venous valves. *J Vasc Surg Venous Lymphat Disord*. 2016;4:329–335. doi: 10.1016/j.jvsv.2015.09.005.
40. Moraczewski T, Tang H, Shapley NC. Flow of a concentrated suspension through an abrupt axisymmetric expansion measured by nuclear magnetic resonance imaging. *J Rheol*. 2005;49:1409–1428.
41. Braekkan SK, Mathiesen EB, Njølstad I, Wilsgaard T, Hansen JB. Hematocrit and risk of venous thromboembolism in a general population. The Tromso study. *Haematologica*. 2010;95:270–275. doi: 10.3324/haematol.2009.008417.
42. Whelihan MF, Zachary V, Orfeo T, Mann KG. Prothrombin activation in blood coagulation: the erythrocyte contribution to thrombin generation. *Blood*. 2012;120:3837–3845. doi: 10.1182/blood-2012-05-427856.
43. Walton BL, Lehmann M, Skorczewski T, et al. Elevated hematocrit enhances platelet accumulation following vascular injury. *Blood*. 2017;129:2537–2546. doi: 10.1182/blood-2016-10-746479.
44. Aleman MM, Byrnes JR, Wang JG, Tran R, Lam WA, Di Paola J, Mackman N, Degen JL, Flick MJ, Wolberg AS. Factor XIII activity mediates red blood cell retention in venous thrombi. *J Clin Invest*. 2014;124:3590–3600. doi: 10.1172/JCI75386.
45. Byrnes JR, Duval C, Wang Y, Hansen CE, Ahn B, Mooberry MJ, Clark MA, Johnsen JM, Lord ST, Lam WA, Meijers JC, Ni H, Ariëns RA, Wolberg AS. Factor XIIIa-dependent retention of red blood cells in clots is mediated by fibrin α-chain crosslinking. *Blood*. 2015;126:1940–1948. doi: 10.1182/blood-2015-06-652263.
46. Cines DB, Lebedeva T, Nagaswami C, Hayes V, Massefski W, Litvinov RI, Rauova L, Lowery TJ, Weisel JW. Clot contraction: compression of erythrocytes into tightly packed polyhedra and redistribution of platelets and fibrin. *Blood*. 2014;123:1596–1603. doi: 10.1182/blood-2013-08-523860.
47. Goel MS, Diamond SL. Adhesion of normal erythrocytes at depressed venous shear rates to activated neutrophils, activated platelets, and fibrin polymerized from plasma. *Blood*. 2002;100:3797–3803. doi: 10.1182/blood-2002-03-0712.
48. Alshehri OM, Hughes CE, Montague S, Watson SK, Frampton J, Bender M, Watson SP. Fibrin activates GPVI in human and mouse platelets. *Blood*. 2015;126:1601–1608. doi: 10.1182/blood-2015-04-641654.
49. Mammadova-Bach E, Ollivier V, Loyau S, Schaff M, Dumont B, Favier R, Freyburger G, Latger-Cannard V, Nieswandt B, Gachet C, Mangin PH, Jandrot-Perrus M. Platelet glycoprotein VI binds to polymerized fibrin and promotes thrombin generation. *Blood*. 2015;126:683–691. doi: 10.1182/blood-2015-02-629717.
50. Riedl J, Kaider A, Marosi C, Prager GW, Eichelberger B, Assinger A, Pabinger I, Panzer S, Ay C. Decreased platelet reactivity in patients with cancer is associated with high risk of venous thromboembolism

and poor prognosis. *Thromb Haemost*. 2017;117:90–98. doi: 10.1160/TH16-02-0123.
51. Reitsma PH, Versteeg HH, Middeldorp S. Mechanistic view of risk factors for venous thromboembolism. *Arterioscler Thromb Vasc Biol*. 2012;32:563–568. doi: 10.1161/ATVBAHA.111.242818.
52. Heestermans M, Salloum-Asfar S, Salvatori D, Laghmani el H, Luken BM, Zeerleder SS, Spronk HM, Korporaal SJ, Wagenaar GT, Reitsma PH, van Vlijmen BJ. Role of platelets, neutrophils, and factor XII in spontaneous venous thrombosis in mice. *Blood*. 2016;127:2630–2637. doi: 10.1182/blood-2015-10-672766.
53. Brill A, Fuchs TA, Savchenko AS, Thomas GM, Martinod K, De Meyer SF, Bhandari AA, Wagner DD. Neutrophil extracellular traps promote deep vein thrombosis in mice. *J Thromb Haemost*. 2012;10:136–144. doi: 10.1111/j.1538-7836.2011.04544.x.
54. Jordan SW, Chaikof EL. Simulated surface-induced thrombin generation in a flow field. *Biophys J*. 2011;101:276–286. doi: 10.1016/j.bpj.2011.05.056.

Highlights

- A miniaturized model of a venous valve was created with dynamic and dimensional similarity to human valves.
- Flow patterns in model valves include primary and secondary vortices in the valve sinus.
- Red blood cells promote transport of platelets into the primary vortex and subsequent adhesion to fibrin formed in the valve pocket.
- Platelet adhesion to fibrin and activation through glycoprotein VI are essential for thrombus propagation out of the valve sinus.

Arteriosclerosis, Thrombosis, and Vascular Biology

JOURNAL OF THE AMERICAN HEART ASSOCIATION

Platelets Drive Thrombus Propagation in a Hematocrit and Glycoprotein VI–Dependent Manner in an In Vitro Venous Thrombosis Model

Marcus Lehmann, Rogier M. Schoeman, Patrick J. Krohl, Alison M. Wallbank, Joseph R. Samaniuk, Martine Jandrot-Perrus and Keith B. Neeves

Arterioscler Thromb Vasc Biol. 2018;38:1052-1062; originally published online February 22, 2018;
doi: 10.1161/ATVBAHA.118.310731
Arteriosclerosis, Thrombosis, and Vascular Biology is published by the American Heart Association, 7272 Greenville Avenue, Dallas, TX 75231

Print ISSN: 1079-5642. Online ISSN: 1524-4636

Platelets drive thrombus propagation in a hematocrit and glycoprotein VI dependent manner in an in vitro venous thrombosis model

Marcus Lehmann, Rogier M. Schoeman, Patrick J. Krohl, Alison M. Wallbank, Joseph R. Samaniuk, Martine Jandrot-Perrus, and Keith B. Neeves

Materials

Bovine serum albumin (BSA), calcium chloride, magnesium chloride, sodium chloride, hydrochloric acid, HEPES, glucose, Fluorinert FC-40, 3,3'-dihexyloxacarbocyanine iodide ($DiOC_6$), acetone, and ethanol were from Sigma Aldrich (St. Louis, MO, USA). Sylgard 184 Silicone Elastomer Kit was from Krayden (Westminster, CO). Innovin lipidated tissue factor (TF) was from Dade-Behring (#10445705, Miami, FL). KMPR 1050 and KMPR 1010 were from MicroChem Corporation (Westborough, MA). Human fibrinogen was from Enzyme Research Laboratory (South Bend, IN) and labeled with Alexa-555 labeling kit purchased from Life Technologies (Grand Island, NY). (Tridecafluoro-1,1,2,2-tetrahydrooctyl)trichlorosilane was from Gelest (SIT8174.0, Morrisville, PA). Annexin V binding buffer (Cat #422201) and Pacific Blue Annexin V label (Cat # 640918) were from Biolegend (San Diego, CA). Abciximab was a gift from the University of Colorado Hospital. Atopaxar was from Adooq Biosciences (Cat #A13813, Irvine, CA). Human D-dimer was from Abcam (Cat #ab98311, Cambridge, MA). ACT017, a GPVI blocking humanized Fab fragment was a gift from Anticor Biotech (Paris, France). 3 µm FITC-labeled polystyrene beads (PSF-003UM) were from Magsphere (Pasadena, CA). Cover glass and plastic syringes (60 mL, BD, Cat #309653 and 3 mL BD, Cat #309657) were purchased from Fisher Scientific (Waltham, MA, Cat # 12-544-18). Biopsy punches, 0.75 mm and 1.5 mm, were from World Precision Instruments (Sarasota, FL, Cat #504529) and Ted Pella (Redding, CA, Cat #15110-15), respectively. Small tubing (Tygon S-54-HL PVC Medical Tubing, 0.010" ID, Tygon S-54-HL PVC Medical Tubing, 0.03" ID) was from Cole Parmer (Vernon Hills, IL). Connectors (1/16" T Type, Cat# 64028) and large tubing (1/16 " ID, Cat #57739) were from US plastics (Lima, Ohio). The 500 µL gastight glass syringe was from Hamilton (Reno, NV, # 81220). 10X HEPES Buffered Saline (HBS) was prepared by dissolving 1500 mM NaCl and 250 mM HEPES in deionized (18.2 MΩ-cm) water. 10X HBS was diluted to 1X using deionized water prior to use. RBC wash buffer (10 mM HEPES, 140 mM NaCl, 1 % w/w glucose, pH =7.3) was made in house. Recalcification buffer (75 mM $CaCl_2$, 37 mM $MgCl_2$ pH= 7.4 in HBS) was made in house. Normal pooled plasma (NPP) was from George King Biomedical (Overland Park, KS, Cat #0010-5).

Microfluidic device fabrication

Two consecutive layers of KMPR 1050 (MicroChem, Newton, MA) photoresist were spun at 1500 rpm on a silicon wafer, with a 20 min soft bake (100 °C) following each spin coat. The photoresists was exposed to a UV light dose of 2608 mJ/cm^2, followed by a 3 min hard bake (100 °C) and development in 2.38% tetramethylammonium hydroxide (AZ MIF 300). The device height was measured with profilometry to be 145 µm. Wafers were pretreated with (tridecafluoro-1,1,2,2-tetrahydrooctyl)trichlorosilane for four hours prior via vapor deposition under vacuum before each molding. PDMS was poured on the wafer at a 10:1 ratio of base to catalyst and the wafer was cured in a convection oven for 4 h at 60 °C. The mold was peeled and inlet and outlet holes (0.75 mm) and a vacuum hole (1.5 mm) were defined with biopsy punches. The PDMS device was cleaned with successive sonication in 1 M HCl, acetone, and ethanol for 5 min each followed by a

forced air dry. The device was placed in a 60 °C oven overnight to fully dry. It was then covalently bonded to cover glass via oxygen plasma (100W, 45 seconds) and then placed in a 60 °C oven overnight.

Supplemental Tables

Supplemental Table I. Flow rates as a function of hematocrit and Re for plasma as the bulk fluid.

Plasma	HCT 0	HCT 0.2	HCT 0.4	HCT 0.6
Re = 0.1	1.5 µL/min	2.3 µL/min	3.7 µL/min	5.9 µL/min
Re = 1	15 µL/min	23 µL/min	37 µL/min	59 µL/min
Re = 10	148 µL/min	235 µL/min	372 µL/min	592 µL/min*
Re = 25	370 µL/min	586 µL/min	930 µL/min	1479 µL/min

* For thrombus formation experiments the HCT 0.6 case was run at 372 µL/min due to volume constraints.

Supplemental Table II. Flow rates as a function of hematocrit and Re for buffer as the bulk fluid.

Buffer	HCT 0	HCT 0.2	HCT 0.4	HCT 0.6
Re = 0.1	0.9 µL/min	1.3 µL/min	2.0 µL/min	3.3 µL/min
Re = 1	9 µL/min	13 µL/min	20 µL/min	33 µL/min
Re = 10	90 µL/min	135 µL/min	204 µL/min	329 µL/min
Re = 25	225 µL/min	337 µL/min	509 µL/min	821.7 µL/min

Supplemental Figures

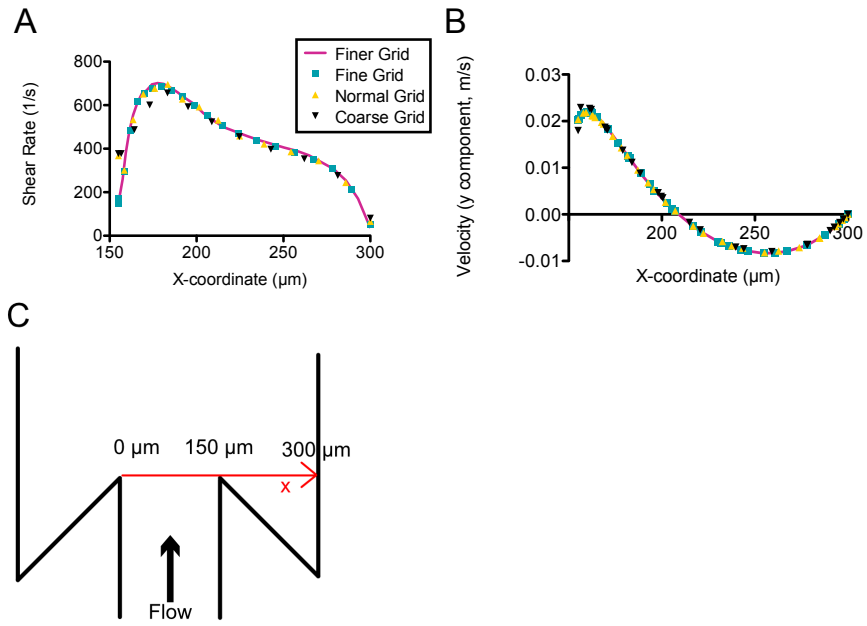

Supplemental Figure I. Wall shear rate (A) and velocity in the direction of bulk flow (B) plotted from the expansion point to the wall for the 150° expansion at Re = 10 for different mesh sizes. The coarse grid results deviate at the edges, but the other results show good agreement. (C) Schematic of the computational geometry including x-axis corresponding to (A) and (B). Note shear rates and velocity in (A) and (B) correspond to the line defined by the expansion point (x = 150 μm) to the wall (x = 300 μm).

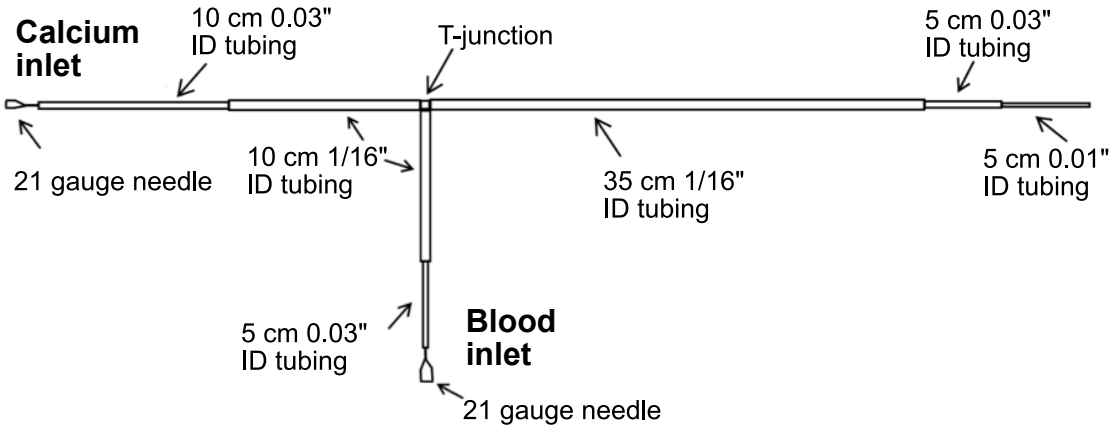

Supplemental Figure II. Tubing connection setup. Lengths and tubing diameters are listed.

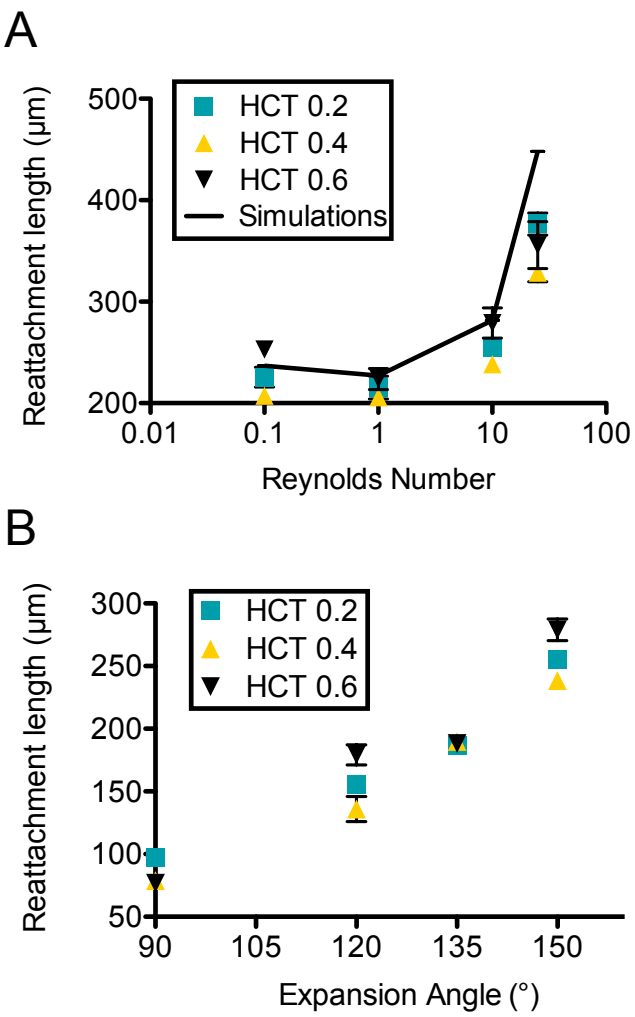

Supplemental Figure III. (A) The flow reattachment length as a function of Re measured experimentally at HCT 0.2, 0.4, and 0.6, as well as from the simulations for the 150° expansion angle. (B) The flow reattachment length at Re = 10 for HCT 0.2, 0.4, and 0.6 as a function of expansion angle. Error bars in both plots represent SEM (n = 3).

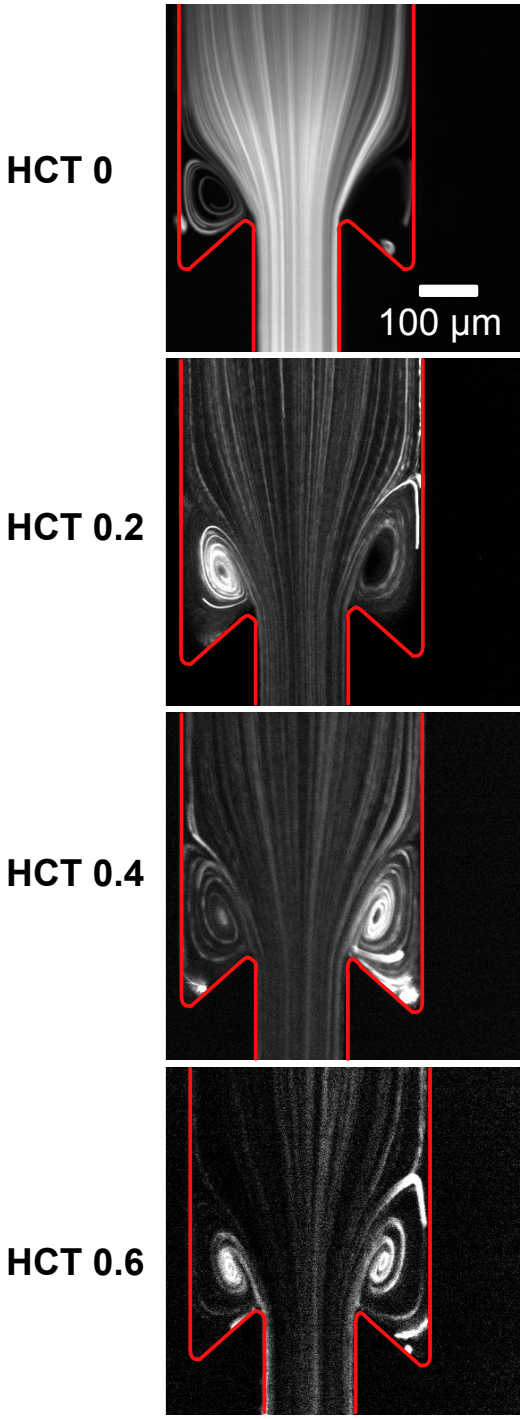

Supplemental Figure IV. Streaklines for the 135° expansion angle at Re = 25 for HCT of 0, 0.2, 0.4 and 0.6.

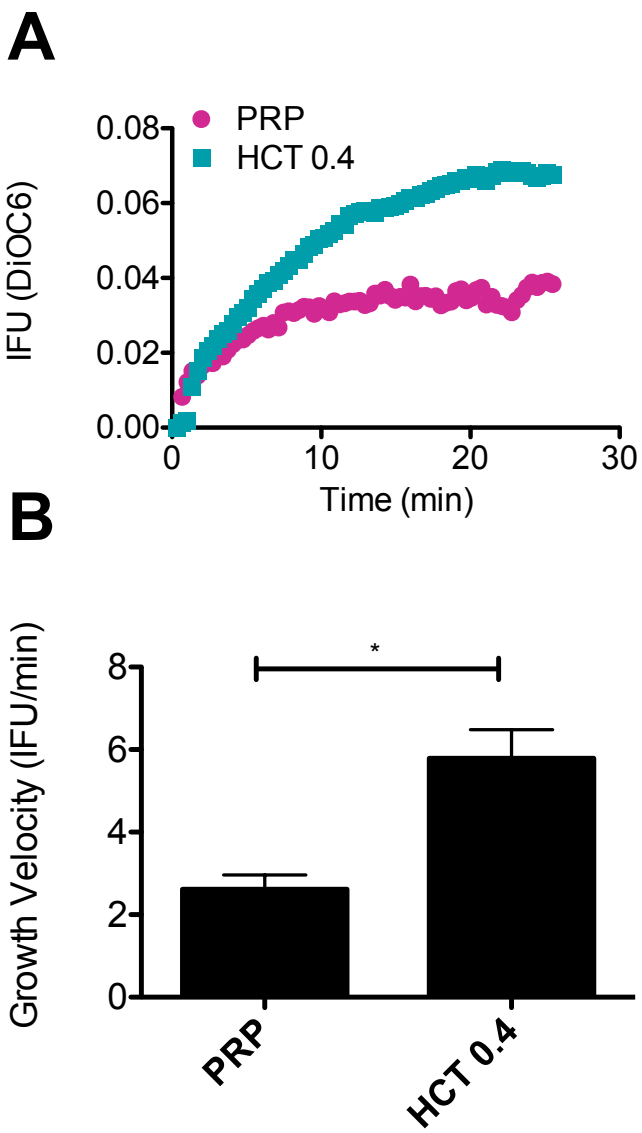

Supplemental Figure V. Platelet accumulation in the valve pocket is increased in the presence of RBC. (A) Characteristic plots of cumulative platelet accumulation in the valve pocket as measured by integrated fluorescence intensity (IFU) if $DiOC_6$ labeled platelets for platelet rich plasma (PRP) and reconstituted blood at HCT 0.4, both at *Re* = *10*. (B) Mean growth velocity of the platelet accumulation for PRP and reconstituted blood. Error bars represent SEM, p = 0.0213 (Mann-Whitney U-test).

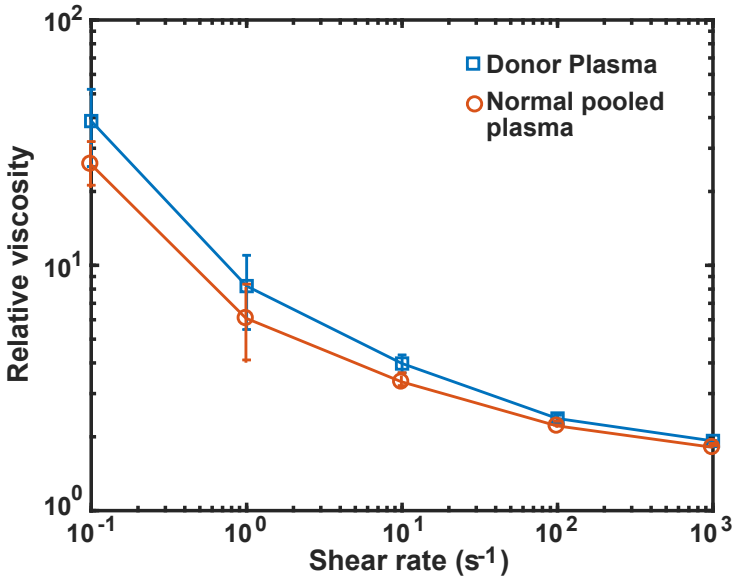

Supplemental Figure VI. Relative viscosity of RBC suspended in autologous donor plasma or normal pooled plasma at a HCT = 0.4. The relative viscosity is the measured suspension viscosity divided by the measured plasma viscosity (no RBC). Each data point represents the average and standard deviation of n = 6 measurements. There was no significant difference (Mann-Whitney U-test) in viscosity at any shear rate between the two suspensions.

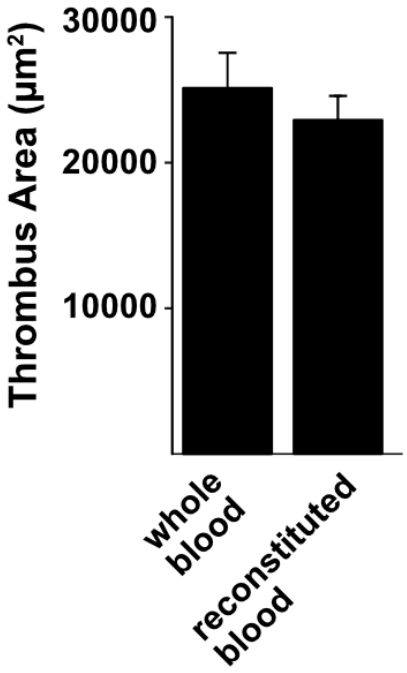

Supplemental Figure VII. Thrombus area at 30 minutes for whole blood from (n = 6 donors, HCT = 0.38-0.51) and reconstituted blood (n = 6 donors, HCT = 0.4) perfused at *Re*= 10 through TF-coated devices. The means and standard errors are plotted. There was no statistical difference as measured by the Mann-Whitney U-test.

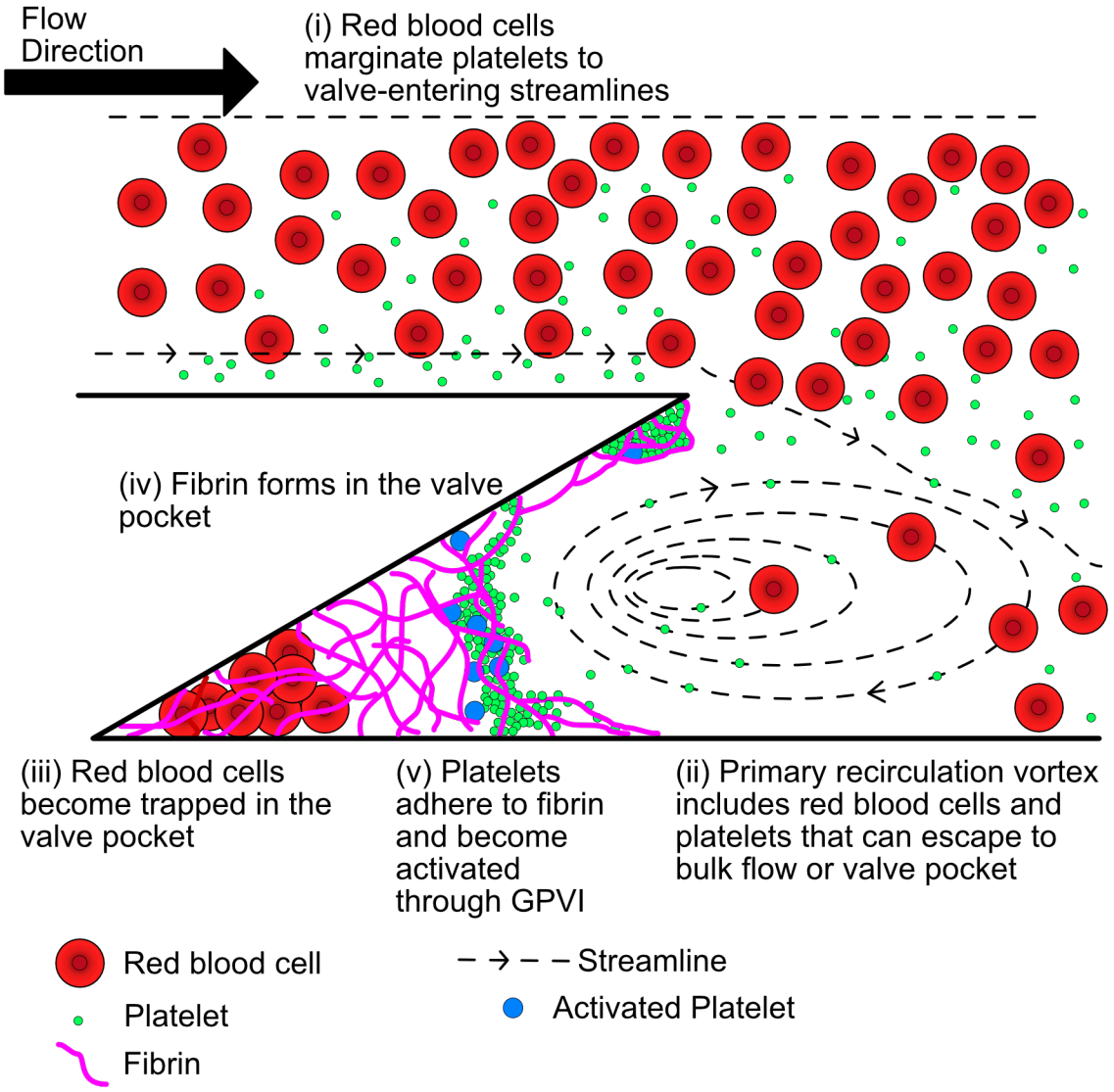

Supplemental Figure VIII. Proposed mechanism of the propagation of the thrombus in the in vitro model. RBC-mediated marginated platelets enter the primary recirculation vortex under hemodynamic conditions that result in flow separation. Fibrin can form in the low shear region of the valve pocket with or without cells. Platelets in the presence of RBC can adhere to and aggregate at the fibrin interface and become activated through GPVI, and for a subpopulation of platelets PS positive. These PS positive platelets provide additional coagulation sites and help propagate the thrombus into the vessel lumen.

Supplemental Video Legends

Supplemental Video 1: Particle streakline timelapse for HCT 0, 0.2 and 0.4 at Re of 1, 10, and 25 for the 150° expansion. Exposure time is 100 ms. Time between frames 1 s.

Supplemental Video 2: Brightfield overview of the thrombus formation at Re = 10, of reconstituted blood (HCT 0.4) through the 150° expansion. RBC are entrapped in the first minutes. The formation of platelet rich and RBC rich regions is visible at 12 minutes.

Supplemental Video 3: Confocal images of the thrombus formation at Re = 10 through the 90° expansion for PRP and reconstituted blood. $DiOC_6$ is in green and labeled fibrin(ogen) is in red.

Supplemental Video 4: Confocal images of the thrombus formation at Re = 10 through the 150° expansion for PNP, PRP, PNP with RBC (HCT 0.4) and reconstituted blood (PRP, HCT 0.4). $DiOC_6$ is in green and labeled fibrin(ogen) is in red. The $DiOC_6$ is absorbed by the PDMS walls, which highlights the geometry even in the absence of platelet adhesion.

Supplemental Video 5: Control confocal images of the thrombus formation at Re = 10 through the 150° expansion for PNP, PRP, PNP with RBC (HCT 0.4) and reconstituted blood (PRP, HCT 0.4) without TF on the surface. $DiOC_6$ is in green and labeled fibrin(ogen) is in red.